Generation of Hyperentangled Photon Pairs

Julio T. Barreiro,[1] Nathan K. Langford,[2] Nicholas A. Peters,[1] and Paul G. Kwiat[1]
[1]*Department of Physics, University of Illinois at Urbana-Champaign, Urbana, Illinois 61801-3080, USA*
[2]*Department of Physics, University of Queensland, Brisbane, Queensland 4072, Australia*
(Received 13 July 2005; published 19 December 2005)

We experimentally demonstrate the first quantum system entangled in *every* degree of freedom (hyperentangled). Using pairs of photons produced in spontaneous parametric down-conversion, we verify entanglement by observing a Bell-type inequality violation in each degree of freedom: polarization, spatial mode, and time energy. We also produce and characterize maximally hyperentangled states and novel states simultaneously exhibiting both quantum and classical correlations. Finally, we report the tomography of a $2 \times 2 \times 3 \times 3$ system (36-dimensional Hilbert space), which we believe is the first reported photonic entangled system of this size to be so characterized.

DOI: 10.1103/PhysRevLett.95.260501 PACS numbers: 03.65.Ud, 03.67.Mn, 42.50.Dv, 42.65.Lm

Entanglement, the quintessential quantum mechanical correlations that can exist between quantum systems, plays a critical role in many important applications in quantum information processing, including the revolutionary one-way quantum computer [1], quantum cryptography [2], dense coding [3], and teleportation [4]. As a result, the ability to create, control, and manipulate entanglement has been a defining experimental goal in recent years. Higher-order entanglement has been realized in multiparticle [5] and multidimensional [6–9] systems. Furthermore, two-component quantum systems can be entangled in every degree of freedom (DOF), or hyperentangled [10]. These systems enable the implementation of 100%-efficient complete Bell-state analysis with only linear elements [11] and techniques for state purification [12]. In addition, hyperentanglement can also be interpreted as entanglement between two higher-dimensional quantum systems, offering significant advantages in quantum communication protocols (e.g., secure superdense coding [13] and cryptography [14]).

Photon pairs produced via the nonlinear optical process of spontaneous parametric down-conversion have many accessible DOF that can be exploited for the production of entanglement. This was first demonstrated using polarization [15,16], but the list expanded rapidly to include momentum (linear [17], orbital [6], and transverse [18] spatial modes), energy time [19] and time bin [20], simultaneous polarization and energy time [21], and recently, simultaneous polarization and 2-level linear momentum [22]. In this work, we produce and characterize pairs of single photons simultaneously entangled in *every* DOF—polarization, spatial mode, and energy time. As observed previously [6], photon pairs from a *single* nonlinear crystal are entangled in orbital angular momentum (OAM). Moreover, polarization entangled states can be created by coherently pumping *two* contiguous thin crystals [23], provided the spatial modes emitted from each crystal are indistinguishable. Finally, the pump distributes energy to the daughter photons in many ways, entangling each pair in energy; equivalently, each pair is coherently emitted over a range of times (within the coherence of the continuous wave pump). We show our two-crystal source can generate a $(2 \times 2 \times 3 \times 3 \times 2 \times 2)$-dimensional hyperentangled state [10], approximately

$$\underbrace{(|HH\rangle + |VV\rangle)}_{\text{polarization}} \otimes \underbrace{(|rl\rangle + \alpha|gg\rangle + |lr\rangle)}_{\text{spatial modes}} \otimes \underbrace{(|ss\rangle + |ff\rangle)}_{\text{energy time}}. \tag{1}$$

Here H (V) represents the horizontal (vertical) photon polarization; $|l\rangle$, $|g\rangle$, and $|r\rangle$ represent the paraxial spatial modes (Laguerre-Gauss) carrying $-\hbar$, 0, and $+\hbar$ OAM, respectively [24]; α describes the OAM spatial-mode balance prescribed by the source [25] and selected via the mode-matching conditions; and $|s\rangle$ and $|f\rangle$, respectively, represent the relative early and late emission times of a pair of energy anticorrelated photons [19].

The most common maximally entangled states are the 2-qubit Bell states: $\Phi^{\pm} = (|00\rangle \pm |11\rangle)/\sqrt{2}$ and $\Psi^{\pm} = (|01\rangle \pm |10\rangle)/\sqrt{2}$, in the logical basis $|0\rangle$ and $|1\rangle$. By collecting only the $\pm\hbar$ OAM state of the spatial subspace, the state (1) becomes a tensor product of three Bell states $\Phi^+_{\text{poln}} \otimes \Phi^+_{\text{spa}} \otimes \Phi^+_{\text{t-e}}$. As a preliminary test of the hyperentanglement, we characterized the polarization and spatial-mode subspaces by measuring the entanglement (characterized by tangle T [26]), the mixture (characterized by linear entropy $S_L(\rho) = \frac{4}{3}[1 - \text{Tr}(\rho^2)]$ [27]), and the fidelity $F(\rho, \rho_t) \equiv (\text{Tr}(\sqrt{\sqrt{\rho_t}\rho\sqrt{\rho_t}}))^2$ of the measured state ρ with the target state $\rho_t = |\psi_t\rangle\langle\psi_t|$. We consistently measured high-quality states with tangles, linear entropies, and fidelities with Φ^+ of $T = 0.99(1)$, $S_L = 0.01(1)$, and $F = 0.99(1)$ for polarization; and $T = 0.96(1)$, $S_L = 0.03(1)$, and $F = 0.95(1)$ for spatial mode, significantly higher than earlier results [18].

The experiment is illustrated in Fig. 1. A 120 mW 351 nm Ar^+ laser pumps two contiguous β-barium borate (BBO) nonlinear crystals with optic axes aligned in perpendicular planes [23]. Each 0.6 mm thick crystal is phase matched to produce type-I degenerate photons at 702 nm into a cone of 3.0° half-opening angle. The first (second) crystal produces pairs of horizontally (vertically) polarized photons, and these two possible down-conversion processes are coherent, provided the spatial modes emitted from each crystal are indistinguishable. With the pump focused to a waist at the crystals, this constraint can be satisfied by using thin crystals and "large" beam waists (large relative to the mismatch in the overlap of the down-conversion cones from each crystal [23]). However, the OAM entanglement is maximized by balancing the relative populations of the low-valued OAM eigenstates [25], which requires smaller beam waists to image a large area of the down-conversion cones. Here we compromise by employing an intermediate waist size ($\sim 90\ \mu$m) at the crystal. Mode-matching lenses are then used to optimize the coupling of the rapidly diverging down-conversion modes into single-mode collection fibers.

The measurement process consists of three stages of local state projection, one for each DOF. At each stage, the target state is transformed into a state that can be discriminated from the other states with high accuracy. Specifically, computer-generated phase holograms [28] transform the target spatial mode into the pure Gaussian (or 0-OAM) mode, which is then filtered by the single-mode fiber [6] [Fig. 1(b)]. After a polarization controller to compensate for the fiber birefringence, wave plates transform the target polarization state into horizontal, which is filtered by a polarizer [Fig. 1(d)]. The analysis of the energy-time state is realized by a Franson-type [19] polarization interferometer without detection postselection [21]. The matched unbalanced interferometers give each photon a fast $|f\rangle$ and slow $|s\rangle$ route to its detector. Our interferometers consisted of $L \sim 11$ mm quartz birefringent elements, which longitudinally separated the horizontal and vertical polarization components by $\Delta n_{\mathrm{quartz}} L \sim 100\ \mu$m, more than the single-photon coherence length ($\lambda^2/\Delta\lambda \sim 50\ \mu$m with $\Delta\lambda = 10$ nm from the interference filters) but much less than the pump-photon coherence length

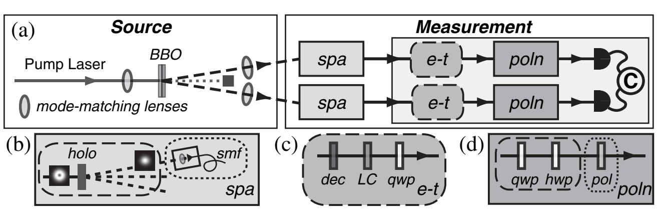

FIG. 1. Experimental setup for the creation and analysis of hyperentangled photons. (a) The photons, produced using adjacent nonlinear crystals (BBO), pass through a state filtration process for each DOF before coincidence detection. The measurement insets show the filtration processes as a transformation of the target state (dashed box) and a filtering step to discard the other components of the state (dotted box). (b) *Spatial filtration (spa)*: hologram (holo) and single-mode fiber (smf). (c) *Energy-time transformation (e-t)*: thick quartz decoherer (dec) and liquid crystal (LC). (d) *Polarization filtration (poln)*: quarter-wave plate (qwp), half-wave plate (hwp), and polarizer (pol).

(~ 10 cm). We rely on the photons' polarization entanglement $|HH\rangle + |VV\rangle$ to thus project onto a two-time state ($|Hs, Hs\rangle + e^{i(\delta_1+\delta_2)}|Vf, Vf\rangle$), where δ_1 and δ_2 are controlled by birefringent elements (liquid crystals and quarter-wave plates) in the path of each photon [21]. Finally, by analyzing the polarization in the $\pm 45°$ basis, we erase the distinguishing polarization labels and can directly measure the coherence between the $|ss\rangle$ and $|ff\rangle$ terms, arising from the energy-time entanglement.

To verify quantum mechanical correlations, we tested every DOF against a Clauser-Horne-Shimony-Holt (CHSH) Bell inequality [29]. The CHSH inequality places constraints ($S \leq 2$) on the value of the Bell parameter S, a combination of four two-particle correlation probabilities using two possible analysis settings for each photon. If $S > 2$, no separable quantum system (or local hidden variable theory) can explain the correlations; in this sense, a Bell inequality acts as an "entanglement witness" [30]. To measure the strongest violation for the polarization and spatial-mode DOFs, we determined the optimal measurement settings by first tomographically reconstructing the 2-qubit subspace of interest; we employ a maximum likelihood technique to identify the density matrix most consistent with the data [27].

Table I shows the Bell parameters measured for the polarization, spatial-mode, and energy-time subspaces, with various projections in the complementary DOF. We see that for every subspace, the Bell parameter exceeded the classical limit of $S = 2$ by more than 20 standard deviations (σ), verifying the hyperentanglement. For both the polarization and spatial-mode measurements, we traced over the energy-time DOF by not projecting in this subspace. We measured the polarization correlations while projecting the spatial modes into the orthogonal basis states ($|l\rangle$, $|g\rangle$, and $|r\rangle$), as well as the superpositions $|h\rangle \equiv (|l\rangle + |r\rangle)/\sqrt{2}$ and $|v\rangle \equiv (|l\rangle - |r\rangle)/\sqrt{2}$). The measured Bell parameters agreed (within $\sim 2\sigma$) with predictions from tomographic reconstruction and violated the inequality by more than 30σ. In the spatial-mode DOF, the corre-

TABLE I. Bell parameter S showing CHSH-Bell inequality violations in every degree of freedom. The local realistic limit ($S \leq 2$) is violated by the number of standard deviations shown in brackets, determined by counting statistics.

	Spatial-mode projected subspaces				
DOF	$\|gg\rangle\langle gg\|$	$\|rl\rangle\langle rl\|$	$\|lr\rangle\langle lr\|$	$\|hh\rangle\langle hh\|$	$\|vv\rangle\langle vv\|$
Φ^+_{poln}	2.76[76σ]	2.78[46σ]	2.75[44σ]	2.81[40σ]	2.75[33σ]
$\Phi^+_{\mathrm{t-e}}$	2.78[77σ]	2.80[40σ]	2.80[40σ]	2.72[30σ]	2.74[29σ]

	Polarization projected subspaces		
DOF	No polarizers	$\|HH\rangle\langle HH\|$	$\|VV\rangle\langle VV\|$
Φ^+_{spa}	2.78[78σ]	2.80[36σ]	2.79[37σ]
$\alpha\|gg\rangle + \|rl\rangle$	2.33[55σ]	2.30[25σ]	2.38[30σ]
$\alpha\|gg\rangle + \|lr\rangle$	2.28[47σ]	2.26[20σ]	2.31[26σ]

lations for the state Φ^+_{spa} were close to maximal ($S = 2\sqrt{2} \approx 2.83$), also in agreement with predictions from the measured state density matrix. In addition, we tested Bell inequalities for nonmaximally entangled states in the OAM subspace: $\alpha|gg\rangle + |rl\rangle$ and $\alpha|gg\rangle + |lr\rangle$; the measured Bell parameters in this case were slightly smaller (5%, maximum) than predictions from tomographic reconstruction [31], yet still 20σ above the classical limit. Finally, our measured Bell violation for the energy-time DOF using particular phase settings is in good agreement with the prediction ($S = 2\sqrt{2}V$) from the measured 2-photon interference visibility $V = 0.985(2)$.

The polarization and spatial-mode state was fully characterized via tomography [27]. We performed the 1296 linearly independent state projections required for a full reconstruction in the $(2 \otimes 3) \otimes (2 \otimes 3)$ Hilbert space consisting of two polarization and three OAM modes for each photon. The measured state (Fig. 2) overlaps the anticipated state [polarization and spatial DOFs of Eq. (1)] with a fidelity of 0.69(1) for $\alpha = 1.88e^{0.16i\pi}$ (numerically fitted), and $S_L = 0.46(1)$, suggesting the difference arises mostly from mixture. Treating the photon pairs as a six-level two-particle system, we can quantify the entanglement using the negativity N [32]. In this $6 \otimes 6$ Hilbert space, N ranges from 0 (for separable states) to 5 (for maximally entangled states), and the fitted state above has $N \approx 4.44$. Our measured partially mixed state has $N = 2.96(4)$, indicating strong entanglement. The spatial mode alone has $N = 1.14(2)$, greater than the maximum ($N = 1$) of any two-qubit system. Thus, our large state possesses 2-qubit and 2-qutrit entanglement.

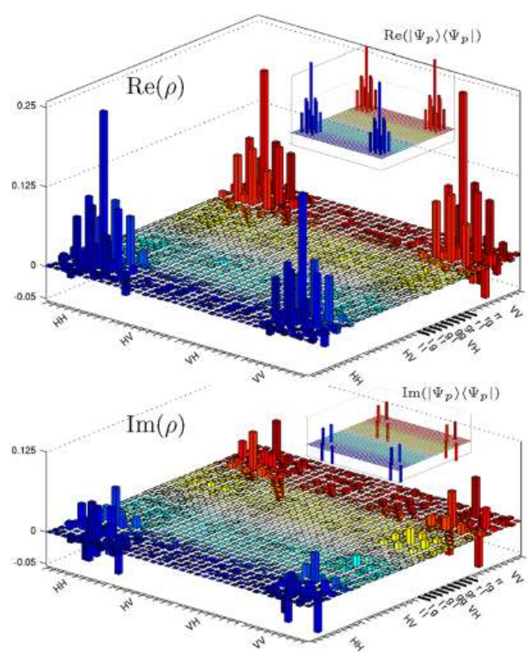

FIG. 2 (color online). Measured density matrix (ρ) and close pure state [$|\Psi_p\rangle \sim \Phi^+_{\text{poln}} \otimes (|lr\rangle + \alpha|gg\rangle + |rl\rangle)$ with $\alpha = 1.88e^{0.16i\pi}$] of a $(2 \times 2 \times 3 \times 3)$-dimensional state of 2-photon polarization and spatial mode [35].

We also selected a state [neglecting the $|gg\rangle$ component, Fig. 3(a)] maximally entangled in both polarization and spatial mode that had $F = 0.974(1)$ with the target $\Phi^+_{\text{poln}} \otimes$

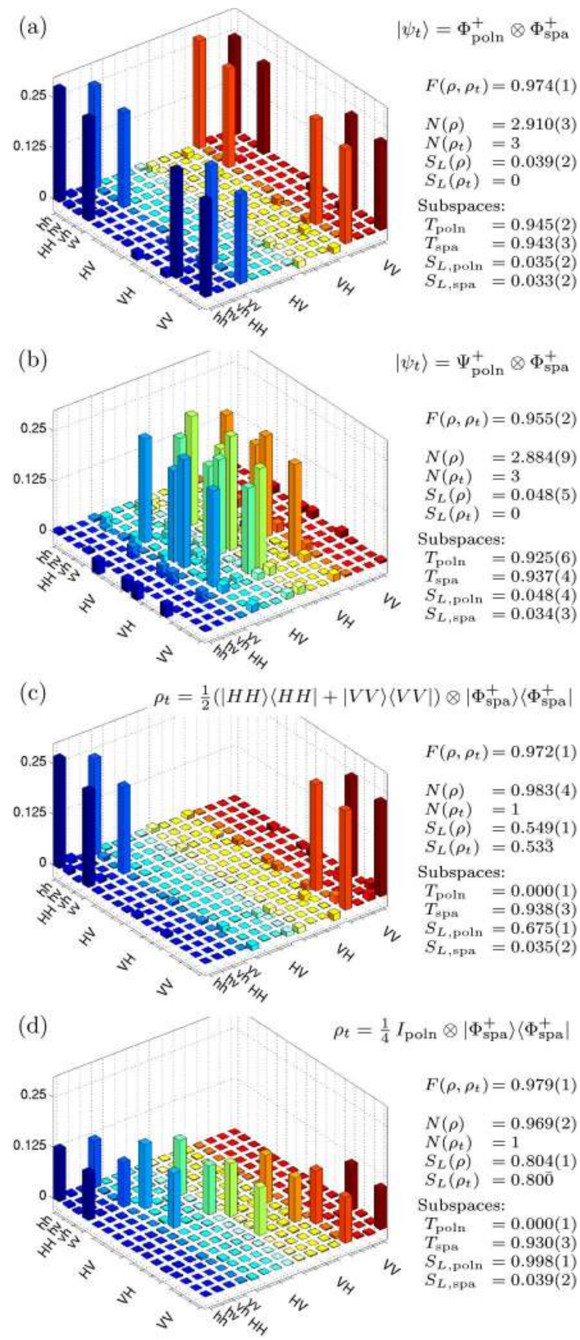

FIG. 3 (color online). Measured density matrices (real parts) of $(2 \times 2 \times 2 \times 2)$-dimensional states of 2-photon polarization and $(+1, -1)$-qubit OAM [35]. For each state, we list the target state ρ_t, the fidelity $F(\rho, \rho_t)$ of the measured state ρ with the target ρ_t, their negativities and linear entropies, and the tangle and linear entropy for each subspace. The negativity for two-qubit states is the square root of the tangle. The magnitudes of all imaginary elements, not shown, are less than 0.03.

Φ^+_{spa}. By tracing over polarization (spatial mode), we look at the measured state in the spatial-mode (polarization) subspaces. The reduced states in both DOFs are pure ($S_L < 0.04$) and highly entangled ($T > 0.94$).

With this precise source of hyperentanglement, we have the flexibility to prepare nearly arbitrary polarization states [33], and to select arbitrary spatial-mode encodings. For example, we also generated a different maximally entangled state: $\Psi^+_{\text{poln}} \otimes \Phi^+_{\text{spa}}$ [Fig. 3(b)]. By coupling to and tracing over the energy-time DOF using quartz decoherers [33], we can add mixture to the polarization subspace, allowing us to prepare a previously unrealized state that simultaneously displays *classical correlations* in polarization and maximal *quantum correlations* between spatial modes [Fig. 3(c)]: $\rho \approx \frac{1}{2}(|HH\rangle\langle HH| + |VV\rangle\langle VV|) \otimes |\Phi^+_{\text{spa}}\rangle\langle\Phi^+_{\text{spa}}|$. We were also able to accurately prepare the state $\rho_t = \frac{1}{4} I_{\text{poln}} \otimes |\Phi^+_{\text{spa}}\rangle\langle\Phi^+_{\text{spa}}|$, with no polarization correlations at all (i.e., completely mixed or unpolarized), while still maintaining near maximal entanglement in the spatial DOF [Fig. 3(d)].

We report the first realization of hyperentanglement of a pair of single photons. The entanglement in each DOF is demonstrated by violations of CHSH-Bell inequalities of greater than 20σ. Also, using tomography we fully characterize a $2 \otimes 2 \otimes 3 \otimes 3$ state, the largest quantum system to date. In restricted $(2 \times 2 \times 2 \times 2)$-dimensional subspace, we prepare a range of target states with unprecedented fidelities for quantum systems of this size, including novel states with a controllable degree of correlation in the polarization subspace. These hyperentangled states enable 100%-efficient Bell-state analysis [11], which is important for a variety of quantum information protocols [3,13]. Because the spatial-mode and energy-time DOFs are infinite in size, we envision examining even larger subspaces, encoding higher-dimensional qudits [7,8]. Finally, we note that the pairwise mechanism of the $\chi^{(2)}$ down-conversion process inherently produces entanglement in photon number [34].

We thank A. G. White and T.-C. Wei for helpful discussions and the ARO/ARDA-sponsored MURI Center for Photonic Quantum Information Systems, the ARC, and the University of Queensland Foundation for support. J. T. B. acknowledges support from CONACYT-México.

[1] R. Raussendorf and H. J. Briegel, Phys. Rev. Lett. **86**, 5188 (2001).

[2] A. K. Ekert, Phys. Rev. Lett. **67**, 661 (1991).

[3] C. H. Bennett and S. J. Wiesner, Phys. Rev. Lett. **69**, 2881 (1992).

[4] C. H. Bennett *et al.*, Phys. Rev. Lett. **70**, 1895 (1993).

[5] Z. Zhao *et al.*, Nature (London) **430**, 54 (2004); P. Walther *et al.*, Nature (London) **434**, 169 (2005).

[6] A. Mair, A. Vaziri, G. Weihs, and A. Zeilinger, Nature (London) **412**, 313 (2001).

[7] R. T. Thew, A. Acín, H. Zbinden, and N. Gisin, Phys. Rev. Lett. **93**, 010503 (2004).

[8] M. N. O'Sullivan-Hale, I. A. Khan, R. W. Boyd, and J. C. Howell, Phys. Rev. Lett. **94**, 220501 (2005).

[9] S. Oemrawsingh *et al.*, Phys. Rev. Lett. **95**, 240501 (2005).

[10] P. G. Kwiat, J. Mod. Opt. **44**, 2173 (1997).

[11] P. G. Kwiat and H. Weinfurter, Phys. Rev. A **58**, R2623 (1998).

[12] C. Simon and J.-W. Pan, Phys. Rev. Lett. **89**, 257901 (2002).

[13] C. Wang *et al.*, Phys. Rev. A **71**, 044305 (2005).

[14] D. Bruss and C. Macchiavello, Phys. Rev. Lett. **88**, 127901 (2002); N. J. Cerf, M. Bourennane, A. Karlsson, and N. Gisin, Phys. Rev. Lett. **88**, 127902 (2002).

[15] Z. Y. Ou and L. Mandel, Phys. Rev. Lett. **61**, 50 (1988).

[16] Y. H. Shih and C. O. Alley, Phys. Rev. Lett. **61**, 2921 (1988).

[17] J. G. Rarity and P. R. Tapster, Phys. Rev. Lett. **64**, 2495 (1990).

[18] N. Langford *et al.*, Phys. Rev. Lett. **93**, 053601 (2004).

[19] J. D. Franson, Phys. Rev. Lett. **62**, 2205 (1989).

[20] J. Brendel, N. Gisin, W. Tittel, and H. Zbinden, Phys. Rev. Lett. **82**, 2594 (1999).

[21] D. V. Strekalov *et al.*, Phys. Rev. A **54**, R1 (1996).

[22] T. Yang *et al.*, Phys. Rev. Lett. **95**, 240406 (2005); C. Cinelli *et al.*, Phys. Rev. Lett. **95**, 240405 (2005).

[23] P. G. Kwiat *et al.*, Phys. Rev. A **60**, R773 (1999).

[24] *Optical Angular Momentum*, edited by L. Allen, S. M. Barnett, and M. J. Padgett (IOP Publishing, Bristol, 2003).

[25] J. P. Torres, A. Alexandrescu, and L. Torner, Phys. Rev. A **68**, 050301 (2003).

[26] W. K. Wootters, Phys. Rev. Lett. **80**, 2245 (1998); $T(\rho) = [\max\{0, \lambda_1 - \lambda_2 - \lambda_3 - \lambda_4\}]^2$, λ_i are the square roots of the eigenvalues of $\rho(\sigma_2 \otimes \sigma_2)\rho^*(\sigma_2 \otimes \sigma_2)$ in nonincreasing order by magnitude, with

$$\sigma_2 = \begin{pmatrix} 0 & -i \\ i & 0 \end{pmatrix}.$$

[27] D. F. V. James, P. G. Kwiat, W. J. Munro, and A. G. White, Phys. Rev. A **64**, 052312 (2001).

[28] Binary plane-wave phase gratings [24] (~40% diffraction efficiency) project the states $|g\rangle$, $|l\rangle$, $|r\rangle$, and $\cos(\theta)|h\rangle + \sin(\theta)|v\rangle = |l\rangle + e^{i2\theta}|r\rangle$ with $\theta = n\pi/8$, $n = -1, 0, \ldots, 8$. By displacing the holograms for $|l\rangle$ ($|r\rangle$) we project arbitrary linear combinations [6] of $|g\rangle$ and $|l\rangle$ ($|r\rangle$).

[29] J. Clauser, M. A. Horne, A. Shimony, and R. A. Holt, Phys. Rev. Lett. **23**, 880 (1969).

[30] B. M. Terhal, Phys. Lett. A **271**, 319 (2000).

[31] Displaced plane-wave holograms allow a small leakage of unwanted states into the fiber [18]. This potentially explains the smaller-than-predicted Bell parameter for the nonmaximally entangled spatial-mode states [e.g., $S_{\text{exp}} = 2.28(1)$ versus the prediction $S_{\text{pred}} = 2.35$].

[32] K. Zyczkowski, P. Horodecki, A. Sanpera, and M. Lewenstein, Phys. Rev. A **58**, 883 (1998).

[33] A. G. White, D. F. V. James, W. J. Munro, and P. G. Kwiat, Phys. Rev. A **65**, 012301 (2002).

[34] H. S. Eisenberg *et al.*, Phys. Rev. Lett. **93**, 193901 (2004).

[35] Data in Fig. 2 (Fig. 3) were collected for 40 s (20 s) per projection with ~600 (~100) detected pairs/s.